Physicochem. Probl. Miner. Process. 52(2), 2016, 620−633

www.minproc.pwr.wroc.pl/journal/

Physicochemical Problems of Mineral Processing

ISSN 1643-1049 (print)
ISSN 2084-4735 (online)

Received August 20, 2015; reviewed; accepted October 21, 2015

QUALITATIVE IDENTIFICATION OF COPPER BEARING MINERALS USING NEAR INFRARED SENSORS

Folorunso Ismail OLUWASEYE[*], Shekwonyadu IYAKWARI[,***], Ambo Amos IDZI[**,***], Okoro Hussein KEHINDE[****], Usman Halima OSU[**]**

[*] Department of Geology and Mineral Sciences, University of Ilorin, Ilorin, Nigeria
[**] Department of Geology and Mining, Nasarawa State University, Keffi, Nigeria
[***] Camborne School of Mines, University of Exeter, Penryn Campus, Cornwall, TR10 9FE, UK
[****] Department of Industrial Chemistry, Material and Environmental-Analytical Research Group, University of Ilorin, Ilorin, Nigeria

Abstract: Application of sensors for on-site fast identification and discrimination of dominant ore bearing particles from associated gangues in a complex ore is an important route in minerals exploration and extraction industries. This paper considers identification and discrimination of copper bearing minerals from associated gangues using near infrared sensors. Different copper bearing minerals in the Akiri copper ore are differentiated on the basis of their near infrared spectra behaviour. The near infrared spectra of individual samples are correlated with their mineralogy and chemistry as analysed by X-Ray diffraction and X-Ray fluorescence equipment, respectively. The obtained results indicated that the detection limit of the near infrared sensor is better than that of both X-ray diffraction and X-ray fluorescence equipment used. Hence, in addition to the minerals identified by the X-ray diffraction equipment, other near infrared active minerals with concentration below the X-ray diffraction detection limit were also detected by the near infrared sensors.

Keywords: *near infrared, exploration, extraction, copper, Akiri*

Introduction

The near infrared (NIR) region of electromagnetic spectrum extending from approximately 750 to 2500 nm contains absorption bands corresponding to C-H, O-H, S-H, and N-H vibrations (Bokobza, 1998; Pasquini, 2003; Li et al., 2008). The advantages of NIR for analysis include speed (ability to analysed rapidly), simplicity of sample preparation, and its non-destructive, non-invasive nature, among others. Its weak sensitivity to minor constituent is its greatest disadvantage (Bokobza, 1998; Iyakwari and Glass, 2015). According to Hunt (1977) NIR spectra are wavelength-intensity records of interaction of electromagnetic (EM) radiation with matter.

http://dx.doi.org/10.5277/ppmp160209

Though a number of minerals could exist within the range of NIR spectrum in varying compositions and arrangements, their identification depends on their individual sensitivity to NIR radiation, concentration and composition in a sample (Iyakwari and Glass, 2015). In the mineral industry especially for preconcentration, Iyakwari and Glass (2015) described NIR as a tool that, when properly applied, can be used to identify minerals qualitatively, optimize recovery as well as save costs of operation.

The aim of this investigation is to establish the suitability of applying the NIR sensors for qualitative identification and individual sample discrimination of the Akiri copper ores. Ten samples were received from Akiri copper mine, which is an arm of the mineralized zone of Middle Benue Trough in Nigeria. Geologically the Akiri deposit is a sedimentary environment. The dominant lithologies in the study area belong to the Eze-Aku formation overlying the Keana formation in the stratigraphy of the middle Benue Trough. The lithologies include sandstones, siltstone, mudstones, shale and conglomeratic ironstone as well as thin limestone beds (Folorunso et al., 2015).

Materials and method

Ten samples were randomly selected from the copper ore samples at Akiri mines, Nasarawa State, North-central Nigeria. Each sample was subjected to various characterization processes outlined in Figure 1.

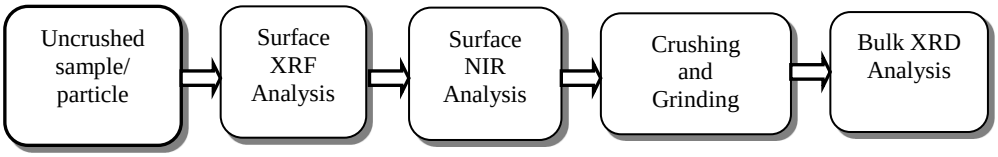

Fig. 1. Stages of sample characterization

First, the elemental composition of the sample surface was measured using a portable desktop thermo scientific Niton FXL 950 FM X-Ray Fluorescence analyser (XRF). The portable XRF (PXRF) analyser employs the energy dispersive spectrometry (EDX) method. The measuring window covers a diameter of 8 mm, and X-rays penetrate approximately 1 to 2 mm into the sample.

On the same solid surface as the PXRF, NIR spectra were generated by a NIR line scanner, which measures on a succession of adjacent areas across the mineral surface, each with a size of 2.9 by 9 mm. The measured NIR signals were converted to a reflectance by first measuring the upper and lower signal values (Iyakwari et al., 2013; Iyakwari and Glass, 2014, 2015). For the upper limit, denoted I_{light}, a highly-reflective board made of aluminium was scanned. For the lower limit, denoted I_{dark}, a scan was

made in the absence of near infrared illumination. The NIR signal, *I*, was then converted into a reflectance, *R*, as follows:

$$R = \frac{I - I_{\text{dark}}}{I_{\text{light}} - I_{\text{dark}}}. \quad (1)$$

Field data are often accompanied by noise self-generated by the sensor and/or the result of physical fluctuation of the surrounding environment (Stark and Lutcher, 2005). All spectra were smoothed using OriginPro 9.0 software with the Savitzky–Golay method (Savitzky and Golay, 1964), applying a polynomial of order 2 to a frame size of 9 points.

For the mineralogical analysis, samples were crushed with a Retsch steel jaw crusher (to -3 mm), then milled to -45 μm using a tungsten-carbide mill. The ground samples were analysed using X-Ray diffraction (XRD, Siemens/Bruker D5000). The XRD measurements were matched with known mineral signatures using EVA software.

Results and Discussion

Ore mineralogy

The XRD analysis performed was qualitative, with a detection limit of 5% and examines samples based on crystallography. Therefore, it cannot detect amorphous material that does not have a crystal structure. It means that minerals identified by the XRD were either above or approximately 5% in concentration in the samples. Therefore, the qualitative XRD only allowed for determination of the most dominant minerals present in the samples (2 – 5 minerals). For each sample on which XRD was performed, determined minerals with known NIR activities showed absorption in the measured NIR spectra, provided that it is dominant and accessible to NIR radiation. It agreed well with findings by Iyakwari and Glass (2015).

According to Gaydon (2010), a rise in the baseline of XRD pattern with increase in the 2-theta value is indicative of the presence of amorphous minerals. Only samples no. 3 and 8 showed this pattern (Table 1). Hence, both samples are thought to contain amorphous minerals, in this case malachite, since it is the common amorphous copper mineral found in the study area (Folorunso et al., 2015)

Major minerals identified by XRD analyses include chalcopyrite, siderite, azurite, quartz, hematite, goethite, pyrite and amorphous phase (malachite) (Table 1). Chalcopyrite, siderite and quartz are the most dominant minerals in the samples in terms of frequency of occurrence, while hematite, azurite, pyrite, and goethite only occurred in one sample each.

Azurite ($Cu_3(CO_3)_2(OH)_2$), siderite (Fe_2CO_3) and malachite ($Cu_2(CO_3)(OH)_2$) are NIR-active minerals in the ore as a function of their functional groups (-OH and CO_3^{2-}) (Hunt, 1979; Iyakwari and Glass, 2015), while siderite contains only the carbonate

radical. Both malachite and azurite contain the carbonate and hydroxyl functional groups. Hematite, chalcopyrite, goethite and pyrite have the ability of masking the spectral absorption features of other minerals (Bishop and Dummel, 1996; Iyakwari et al., 2013; Iyakwari and Glass, 2015). Hence, such minerals are described by Iyakwari and Glass (2015) as non-feature-displaying NIR-active minerals.

The main copper bearing minerals in the ore are chalcopyrite ($CuFeS_2$), azurite and malachite, while hematite (Fe_2O_3), goethite ($FeO(OH)$), siderite (Fe_2CO_3) and pyrite (FeS_2) are iron bearing minerals and quartz (SiO_2) is a silicate.

The XRD analysis indicated that the ore is made up of four major mineral groups, that is sulphide, silicate, carbonates and oxide.

Table 1. Qualitative XRD analysis of the Akiri copper ore samples analysed at Camborne School of Mines (CSM). Presence of a mineral is marked with +. Note that the amorphous phase is only inferred from XRD patterns with rising baselines

Sample ID	Chalcopyrite	Siderite	Azurite	Quartz	Hematite	Goethite	Pyrite	Amorphous Phase (malachite)
1	+	+						
2			+					
3								+
4	+	+		+				
5	+							
6	+	+						
7	+	+		+				
8					+	+		+
9				+			+	
10	+			+				

Ore chemistry

The main objective of this research was to scope a strategy for early identification and discrimination of Cu bearing particles from non-copper bearing particles using the NIR sensors. Since the NIR range used (1300 to 2400 nm) does not sense elemental copper signature(s), but copper bearing mineral (Iyakwari et al., 2013), the NIR spectral interpretation was correlated with elemental data from a portable XRF. This was done to identify samples that contain copper for a 1:1 match. Results obtained from PXRF elemental analysis are presented in Table 2.

Comparing the results of XRD and PXRF (Tables 1 and 2, respectively) the data indicate that samples analysed with XRD, which contain chalcopyrite as copper bearing mineral (sample no. 1, 2, 4, 5, 6, 7 and 10), also show copper values at economic concentration by PXRF. The copper concentration ranges from 0.93% in sample no. 1 to 17.69% in sample no. 2. Samples inferred to contain amorphous mineral phase (malachite) by XRD show no copper by PXRF. This is probably due to

the detection limit of PXRF or sample mode since XRD measured powders, while PXRF was performed on solid samples. Therefore, while XRD samples are liberated to obtain bulk mineralogy, the solid face scanned by PXRF may have copper bearing minerals occurring below the detection limit.

Table 2. PXRF data for Akiri copper ore, values in %, where bdl denotes below detection limit

Sample ID	Mn	Fe	Co	Ni	Cu
1	0.29	13.24	bdl	0.02	0.93
2	bdl	1.34	bdl	bdl	17.69
3	bdl	bdl	bdl	bdl	bdl
4	0.15	8.46	bdl	0.03	1.36
5	0	9.94	0.05	0	4.4
6	0.2	11.26	0.02	0.1	1.25
7	0.2	11.33	bdl	0.01	1.65
8	bdl	bdl	bdl	bdl	bdl
9	0.01	4.04	0.03	bdl	0.07
10	0	4.39	0.04	0	2.84

Though XRD indicated that sample no. 8 contains hematite and goethite, PXRF data show absence of iron in the sample. Unlike sample no. 8, all siderite-bearing samples contain iron (Table 2). The same is true for the pyrite bearing sample no. 9. The results from both analytical methods provided a good correlation.

NIR spectra of Akiri samples

With respect to the bulk ore mineralogy (Table 1), the NIR spectra of minerals were examined with reference to Clark et al. (2003), Iyakwari et al., (2013), Iyakwari and Glass, (2014, 2015). The analysis revealed the ability of malachite, azurite and siderite to show diagnostic features between 1300 to 2400 nm (Table 3). Specifically, malachite show features near 2275 and 2360 nm, azurite shows its diagnostic features near 1500, 1950, 2040, 2270 and 2340 nm, while siderite shows features near 1920, and 2300 nm. Though not detected by XRD analysis, calcite was also included in the study due to its occurrence in association with most copper ore (Robb 2005) and its strong NIR activity (Iyakwari and Glass, 2014). According to Iyakwari and Glass (2014), the spectra of calcite show strong absorption feature near 2340 nm. None of the NIR-active minerals show additional feature(s) near 1400 and or 1900 nm which are indicative of water, when they occur together or when only the -OH at 1400 nm is present (Aines and Rossman, 1984; Clark, 1990; Iyakwari and Glass, 2014).

On the other hand, chalcopyrite, hematite, goethite, and pyrite do not display feature(s) within the 1300 to 2400 nm range used. The inability of these minerals to display features is due to their non-NIR-active functional groups bearing and also due to the presence of iron in their chemical structure, as iron suppresses features of some

minerals (Clark, 1995; Bishop and Dummel 1996; Iyakwari and Glass, 2015). Quartz as a single mineral shows the water NIR absorption feature near 1400 and 1900 nm (Iyakwari et al., 2013). When quartz occur in complex mixtures, the resultant spectra does not show feature indicative of quartz (Iyakwari and Glass, 2015). This is so, since it does not contain the NIR-active functional group. Hence, its ability to show features as a single mineral is as a result of impurities (Iyakwari and Glass, 2014). According to Aines and Rossman (1984), Dalm et al. (2014), Iyakwari and Glass (2014), water is either adsorbed on the mineral surface or part of the mineral crystal structure

Therefore, since none of the constituent minerals contained water within their chemical structure, where water features are present in the spectra of ore particle; such feature(s) will denote impurities.

Table 3. Diagnostic absorption features of NIR -active minerals (between 1300 nm and 2340 nm) in Akiri copper ore (Modified from Iyakwari et al., 2013)

Groups	Mineral	Molecule absorption feature, nm		
		-OH	H_2O	CO_3^{2-}
Silicate	Quartz	-	1415, 1915	-
Sulphide	Chalcopyrite	does not display absorption feature		
	Pyrite			
Carbonate	Calcite	-	-	1920, 2000, 2150, 2340
	Malachite	2360	-	2275, 2360
	Siderite			1920, 2340
	Azurite		-	1500, 1950, 2050, 2290, 2350
Oxide	Hematite	does not display absorption feature		
	Goethite			
	Chalcopyrite			

Individual sample minerals and spectra mapping

Since the NIR range used (1300 to 2400 nm) does not sense copper, but copper bearing minerals (Iyakwari et al., 2013), the copper content of individual samples was obtained from PXRF data (Table 2). The NIR measures each spectrum at a dimension of 0.9x0.29 cm (Iyakwari and Glass, 2015). The size of individual particles was variable, ranging between 1 and 5 cm. Therefore, the number of spectra produced by individual samples is dependent on the particle size. The longest axis of individual samples was aligned perpendicular to the direction of NIR conveyor belt motion. A single linescan was made for each sample on a stationary mode, ensuring that each sample was characterised by 4 to 17 spectra (Figures 1 to 10). The resultant spectra are presented and discussed below, with summary in Table 4.

Sample no. 1 generated seven spectra (Fig. 2). The longest axis has was 2.03 cm. The spectra displayed variable absorption properties. While spectra no. 1, 2, 3, and 7,

appeared flat showing no absorption features, spectra no. 5, 6 and 7 show broad depression near 1900 and 2340 nm. On comparison with sample mineralogy (Table 1) the sample contained chalcopyrite, which is NIR-active but does not display absorption feature(s), and siderite which is a feature displaying NIR-active mineral. Hence, while the depressed spectra lacking defined absorption centre(s) indicated the presence of siderite, the flat spectra showed that chalcopyrite is dominant along the range. According to Iyakwari and Glass (2015) the depression of spectrum lacking defined absorption centres could be due to complex mineralogy or minerals with similar NIR radiation accessibility competing for dominance. Hence, the spectra indicated chalcopyrite dominating siderite by cancelling out its features thereby leaving it broad in spectra no. 5, 6 and 7.

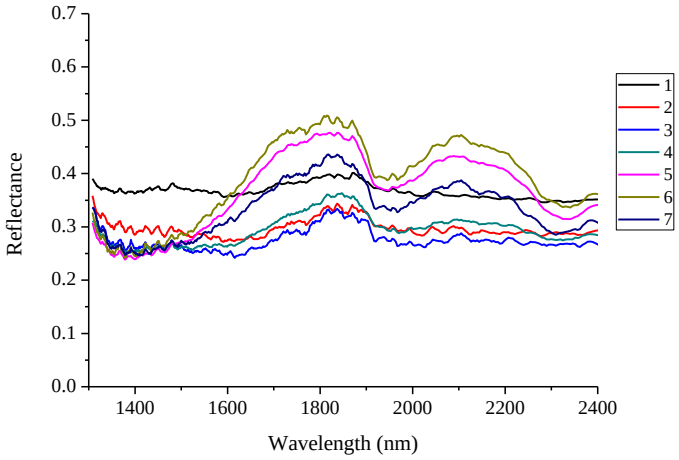

Fig. 2. NIR spectra of sample no. 1

Sample no. 2 produced seven spectra (Fig. 3). All spectra showed absorption features near 1500, 1930, 1980, 2050, 2010, 2290 and 2350 nm. All major absorption features corresponded to the azurite CO_3^{2-} diagnostic features within the longer range of NIR (Table 3). Sample mineralogy indicated that sample was composed dominantly of azurite. Thus, the high copper concentration as shown by PXRF data (Table 2) was from azurite. Hence, the sample provided a 1:1 correlation of XRD, NIR and PXRF.

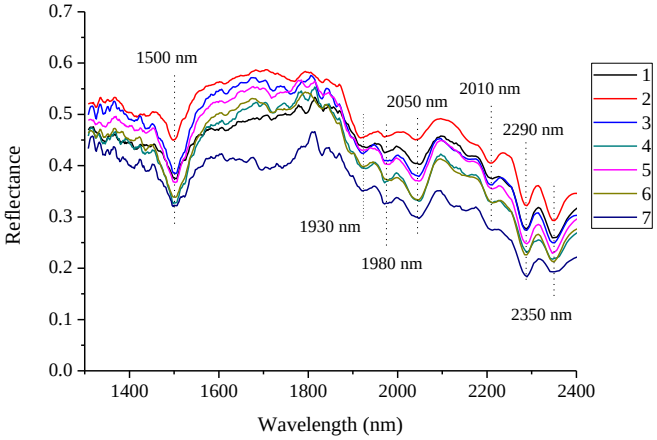

Fig. 3. NIR spectra of sample no. 2

Spectra of sample no. 3 showed absorption features near 2275 and 2360 nm (Fig. 4). All features corresponded to the malachite diagnostic absorption feature within the longer NIR region (Table 3). The presence of malachite is confirmed by the amorphous signatures in samples mineral data (Table 1), where the presence of malachite was denoted as amorphous phase, as inferred from rise in 2-theta pattern. Hence, this agrees with the findings reported by Gaydon (2010). Though the PXRF did not indicate copper in this sample, and malachite is inferred from XRD pattern, the analysis showed that both NIR and XRD were in agreement and had better detection limit than the PXRF. Sample no. 3 generated six spectra, indicating the longest axis is 1.74 cm.

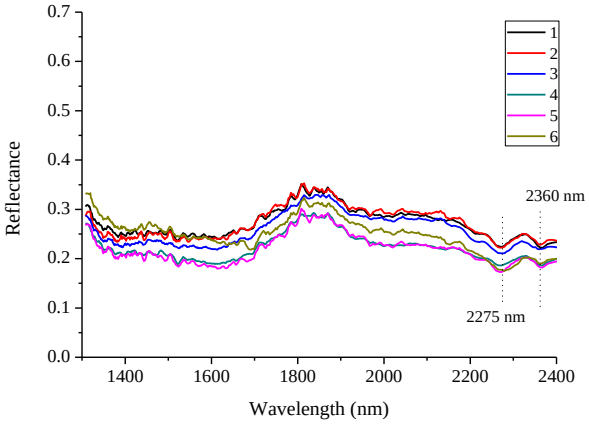

Fig. 4. NIR spectra of sample no. 3

The longest axis of sample no. 4 measured 1.16 cm and produced four spectra (Fig. 5). Of the four spectra, only spectrum no. 1 showed a weak absorption feature near 2340 nm. Feature shown by spectrum no. 1 corresponded to both siderite and calcite. Given that calcite was not detected from the mineralogical analysis, the feature is assigned to siderite. While the lack of absorption features in spectrum no.2, 3 and 4 could be assigned to chalcopyrite. Only chalcopyrite and siderite are the NIR-active minerals detected by XRD analysis of the sample (Table 1). The analysis of sample spectra was in agreement with the XRD mineralogy. Also, the NIR spectra revealed that chalcopyrite was the dominant mineral in the sample.

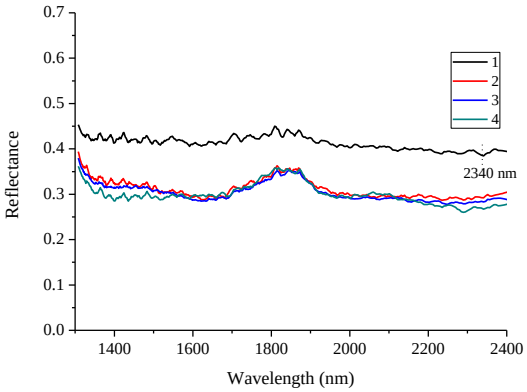

Fig. 5. NIR spectra of sample no. 4

Sample no. 5 generated eight spectra. All spectra showed no absorption features (Fig. 6). The comparison of spectra with mineral data (Table 1) indicated that the sample contained only chalcopyrite as the copper bearing mineral. Hence, the lack of absorption feature(s) in sample can be explained by the presence of chalcopyrite, which is a non-feature displaying NIR-active mineral.

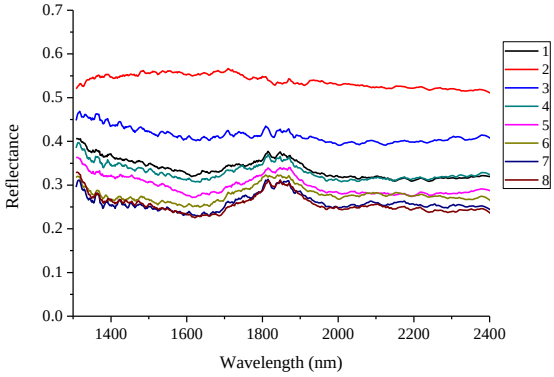

Fig. 6. NIR spectra of sample no. 5

The NIR analysis of sample no. 6 generated seventeen spectra (Fig. 7). Except spectrum no. 17, which showed absorption feature near 2290 nm, the remaining sixteen spectra appeared with no defined absorption feature(s) and in most cases showed broad absorption between 2250 and 2350 nm. Mineral data (Table 1) showed that sample contained chalcopyrite and siderite. The absorption feature displayed by spectrum no. 17 corresponded to one of azurite diagnostic absorption features. The lack of siderite features in the sample indicated that chalcopyrite was more NIR-active and its activity involved masking/broadening of absorption features of other NIR-active features displaying minerals where they occurred together. In most cases such feature masking characteristics may be either concentration or accessibility to NIR radiation dependent (Iyakwari and Glass, 2015). Given that mineral data available is only qualitative, the issue of concentration cannot be confirmed, hence, it shall be assumed that chalcopyrite spectra dominance of siderite is accessibility to radiation dependent. Therefore, though diluted, this is given that the desired mineral (chalcopyrite) dominates the spectrum.

The presence of azurite features in spectrum no. 17, even when it was not detected by the XRD analysis, indicated that NIR had a better detection limit than the XRD. Hence, the concentration of azurite in the sample may be below the 5% detection limit, which is why it was not detected from the XRD analysis.

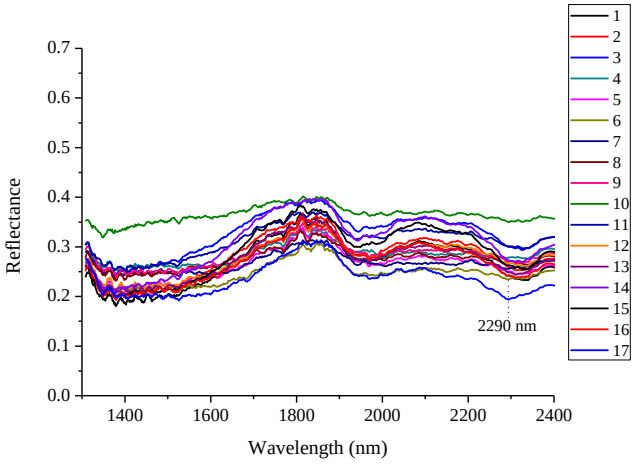

Fig. 7. NIR spectra of sample no. 6

Sample no. 7 generated eleven spectra, all showing broad depression between 2250 and 2350 nm (Fig. 8). Mineral data (Table 1) showed chalcopyrite, siderite and quartz as the minerals detected. Both chalcopyrite and siderite are NIR-active. While siderite displays features, chalcopyrite is known for its feature masking characteristics of other minerals (Iyakwari and Glass, 2015). Hence, chalcopyrite was responsible for the broadness of the spectra of sample no. 7.

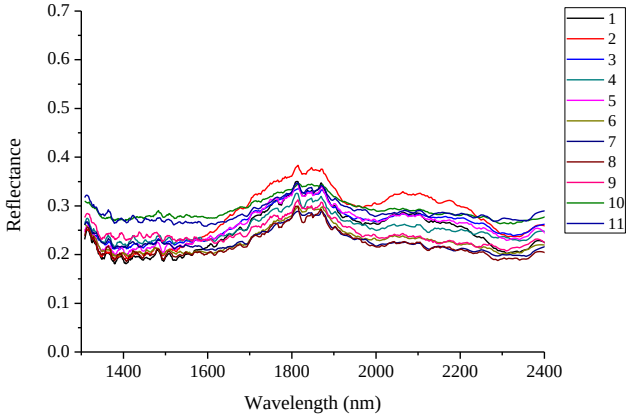

Fig. 8. NIR spectra of sample no. 7

Sample no. 8 generated five spectra (Fig. 9) corresponding to an axial length of 1.54 cm. From the five spectra, only spectra no. 4 and 5 showed no absorption features. Spectra no. 1, 2, and 3 showed the feature near 2275 nm, thus indicative of malachite (Table 3). The presence of malachite features was in agreement with mineral data of the sample (Table 1). Mineral data also indicated hematite and goethite in concentration. Though the presence of hematite could be responsible for the absence of malachite feature near 2360 nm, the 2275 nm feature confirmed that malachite was more NIR-active in the spectra. The spectra dominance of malachite over hematite confirmed finding by Iyakwari and Glass (2015). Similar to what was obtained in sample no. 3, the NIR spectral analysis was in agreement with the assumed presence of amorphous mineral in concentration.

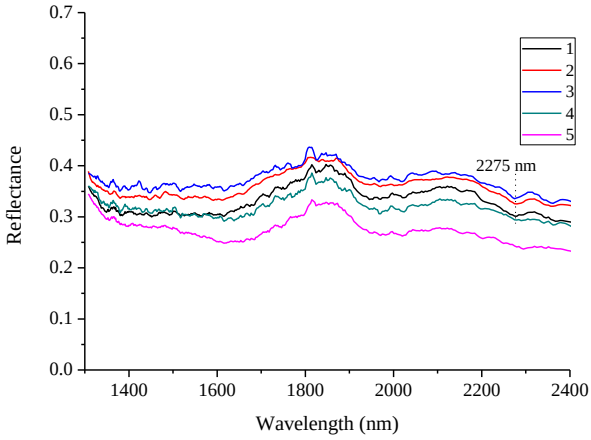

Fig. 9. NIR spectra of sample no. 8

The spectra of sample no. 9 appeared featureless across all wavelength range (Fig. 10). The sample mineral data (Table 1) showed that the sample was composed of quartz and pyrite. Both minerals are non-NIR-active mineral, therefore the lack of features in the spectra of sample no. 9 was observed. The analysis also agrees with the PXRF which shows that the sample does not contain copper. With no knowledge of sample mineralogy, given its lack of absorption features, such sample(s) could easily be misclassified as chalcopyrite bearing one.

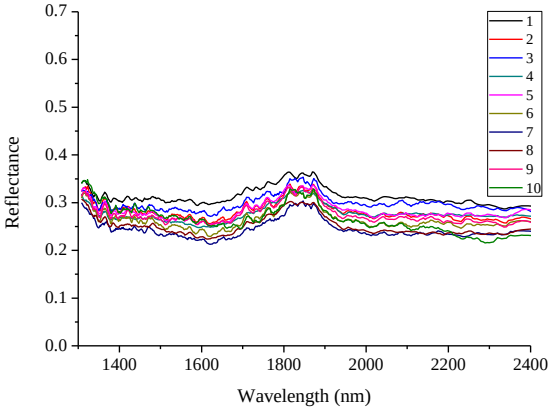

Fig. 10. NIR spectra of sample no. 9

From twelve spectra generated by sample no. 10, all of them appeared without absorption features (Fig. 11). Sample mineral data showed that the sample is composed of chalcopyrite as the only NIR-active mineral. Hence, spectra confirmed the non-feature displaying characteristic of chalcopyrite.

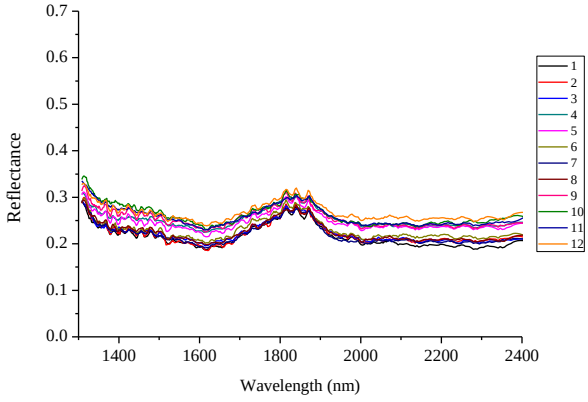

Fig. 11. NIR spectra of sample no. 10

Table 4. Summary of individual particle spectrum and mineral map of sample, where Az – azurite, Ch – chalcopyrite, Ma – malachite, Si – siderite, Hm – hematite

Sample ID	Spectrum number																
	1	2	3	4	5	6	7	8	9	10	11	12	13	14	15	16	17
1	Ch	Ch	Ch	Ch	Si	Si	Si										
2	Az	Az	Az	Az	Az	Az	Az										
3	Ma	Ma	Ma	Ma	Ma	Ma											
4	Si	Ch	Ch	Ch													
5	Ch	Ch	Ch	Ch	Ch	Ch	Ch	Ch									
6	Ch	Ch	Ch	Ch	Ch	Ch	Ch	Ch	Ch	Ch	Ch	Ch	Ch	Ch	Ch	Ch	Az
7	Ch	Ch	Ch	Ch	Ch	Ch	Ch	Ch	Ch	Ch	Ch						
8	Ma	Ma	Ma	Hm	Hm												
9	Ch	Ch	Ch	Ch	Ch	Ch	Ch	Ch	Ch	Ch							
10	Ch	Ch	Ch	Ch	Ch	Ch	Ch	Ch	Ch	Ch	Ch	Ch					

Implications to copper bearing minerals exploration and conclusions

Since NIR is a surface technique, it was assumed that the surface mineral(s) were responsible for the absorption of NIR radiation observed in the spectra of samples. This statement may not be entirely true as it may also depend on the depth of sample penetration and the opacity of the first surface mineral encountered. Unlike the XRD that involved powdered samples to obtain bulk mineralogy, measurement by both NIR and PXRF were taken on unground samples. Hence, it was assumed that the first minerals encountered by the NIR sensor were responsible for the chemistry obtained by PXRF, though the PXRF does not probe as deep as the NIR. Samples no. 3 and 8 showed that the NIR had better depth of sample penetration than the PXRF as it was able to detect the amorphous phase (malachite), while the PXRF did not detect copper in those samples. Though most NIR spectra of samples compared favourably with the XRD, a few samples showed some minerals not detected by the XRD, thus indicating that the NIR had better detection limit.

The result also indicate that NIR is a good tool for on-site determination and discrimination of copper bearing ores from gangues. Therefore, NIR technique could be an important tool for qualitative mineralogical analysis of NIR-active minerals as an indicator before bulk mineralogy of the Akiri copper ore.

It is worthy to note that though some features may be common to more than one mineral, none of two minerals display completely identical absorption spectra. Hence, individual copper bearing minerals were identified and their diagnostic features were used to distinguish them from the non-copper bearing minerals. The discrimination of chalcopyrite from hematite or other feature masking NIR-active minerals was not possible as both minerals had similar spectral behaviour.

References

AINES R.D., ROSSMAN G.R., 1984. *Water in minerals? A peak in the infrared*, J Geophys Res, 89 (B6) 4059-4071.

BISHOP J.L., DUMMEL A., 1996. *The influence of fine-grained hematite powder on the spectral properties of Mars soil analogs; VIS-NIR bi-directional reflectance spectroscopy of mixtures*. Lunar and Planetary Institute Science Conference Abstracts, Vol. 27.

BOKOBZA L., 1998. *Near Infrared Spectroscopy*. J Near Spectrosc, 6, 3-7

CLARK R.N., KING T.V.V., KLEJWA M., SWAYZE G.A., VERGO N., 1990, *High spectral resolution reflectance spectroscopy of minerals*. J. Geophys. Res., 95: 12653–12680.

CLARK R.N., 1995, *Reflectance spectra*. In: Ahrens, T.J. (Ed.), *Rock Physics and Phase: A Handbook of Physical Constants*, Washington, American Geophysical Union, 178–188.

CLARK R.N., SWAYZE G.A., WISE R., LIVO K.E., HOEFEN T.M., KOKALY R.F., SUTLEY S.J., 2003. *USGS Digital Spectral Library splib05a*, U.S. Geological Survey, Open File Report 03-395.

DALM M., BUXTON M.W., VAN RUITENBEEK F.J., VONCKEN J.H., 2014. *Application of near-infrared spectroscopy to sensor based sorting of a porphyry copper ore*. Miner. Eng., 58, 7-16.

FOLORUNSO I.O., BALE R.B., ADEKEYE J.I.D., 2015. *The stratigraphy, petrology and structural evolution of Akiri and its environs, Middle Benue Trough, Nigeria*. Journal of Science, Technology, Mathematics and Education 11(1), 95-108.

HUNT G.R., 1977. *Spectral signatures of particulate minerals in the visible and near-infrared*. Geophys, 42(3), 501–513.

HUNT G.R., 1979. *Near-infrared (1.3-2.4 μm) spectra of alteration minerals; potential for use in remote-sensing*, Geophys., 44 (12) 1974-1986.

IYAKWARI S., GLASS H.J., 2015. *Mineral preconcentration using near infrared sensor-based sorting*, Physicochemical Problems of Mineral Processing 51(2), 661-674

IYAKWARI S., GLASS H.J., 2014. *Influence of mineral particle size and choice of suitable parameters for ore sorting using near infrared sensors*. Miner. Eng., 69, 102-106.

IYAKWARI S., GLASS H. J., KOWALCZUK P.B., 2013. *Potential for near infrared sensor-based sorting of hydrothermally-formed minerals*. J. Near. Infrared Spectrosc., 21(3), 223-229.

LI L., WU Q., LI S., WU P., 2008. *Study of the infrared spectral features of an epoxy curing mechanism*. Appl. Spectrosc. 62(10), 1129-1136.

PASQUINI C., 2003. *Near infrared spectroscopy: fundamentals, practical aspects and analytical applications*. J. Braz. Chem. Soc., 14(2), 198–219.

ROBB L., 2005. *Introduction to ore-forming processes*. Wiley-Blackwell.

SAVITZKY A., GOLAY M.J., 1964. *Smoothing and differentiation of data by simplified least squares procedures*. Anal. chem., 36(8), 1627-1639.

STARK E., LUCHTER K., 2005. *NIR instrumentation technology*. NIR news, 16(7) 13-16.